Asynchronous Mio-Pliocene exhumation of the central Venezuelan Andes

1. Fission-track Methods

Apatite was extracted from rock samples using standard magnetic and heavy liquid techniques. Grains were mounted in epoxy, polished and etched in a 5.5M HNO_3 solution at 20°C for 20 s. All samples were dated using the external detector method, with U-poor mica as external detector and a zeta calibration factor determined with Fish Canyon and Durango age standards. Samples were irradiated at the well-thermalized ORPHEE facility of the *Centre d'Etudes Nucléaires* in Saclay, France, with a nominal fluence of ~5×10^{15} neutrons/cm^2. Neutron fluences were monitored using IRMM540 dosimeter glasses. Mica detectors were etched in 48% HF at 20°C for 18 minutes. All samples were analysed by M.A. Bermúdez. Samples were counted dry with a BH-2 Olympus microscope at 1250× magnification. Separate mounts for each sample were subsequently Cf-irradiated at the University of Melbourne, Australia, in order to reveal sufficient amounts of confined tracks for length measurements. Confined track-length measurements were performed by digitizing the track ends using a drawing tube; the etch-pit width parallel to the C-axis (D_{par}) of 100 tracks crossing the etched internal surface was measured using the same digitizing technique. Apatite fission-track (AFT) data (ages, lengths and D_{par} values) are reported in Table DR1.

2. Numerical thermal-kinematic modeling

Numerical modeling in this work used the 3D thermal evolution code *Pecube* (Braun, 2003), which predicts time-temperature paths for rocks currently at the surface and arbitrary exhumation and relief histories. Time-temperature paths are used to predict ages for different thermochronologic systems. Here, we calculate apatite fission-track (AFT) ages using the forward model of Green et al. (1989), with parameter values as re-evaluated by Stephenson et al. (2006).

In order to assess possible exhumation and relief histories, we couple *Pecube* to an inversion scheme based on the Neighborhood Algorithm (NA) of Sambridge (1999b, a). The NA is a two-stage numerical approach to derive Bayesian estimates on input parameters for non-linear inverse problems (cf. Valla et al., 2010; Glotzbach et al., in review for a recent discussion). The first or sampling stage is an iterative search method, during which sampling gradually concentrates on regions of the multidimensional parameter space where the misfit function is optimized (i.e. sets of parameters values that minimize the misfit to the data). The parameter space is divided into Voronoi cells, centered on each sampled model, that represent the nearest neighborhood about each point. A certain amount of best-fitting forward models (here 50%) is used to define new Voronoi cells and thus to fix a new parameter space. This new parameter space is then sampled during the next iteration in a random fashion, eventually

converging towards one or several sets of parameters that minimize the misfit function to the data, which is calculated as:

$$misfit = 0.5 \cdot \sum_{i=1}^{n} \left(\frac{o_i - p_i}{e_i} \right)^2 \quad (1)$$

where n is the number of observations, o_i and p_i correspond to observed and predicted fission-track age for each sample i, and e_i is the observed error in the age.

Inversions aim at constraining the exhumation history (defined as a number of phases of exhumation, for each of which we search the optimum timing and exhumation rate), thermal structure of the crust (defined by basal temperature and heat production) and, in our initial inversions, relief development (defined as in Valla et al., 2010; cf. Table DR2). However, the AFT age-elevation relationship alone does not constrain relief development in any detail (Valla et al., 2010), so we decided to run further inversions assuming steady-state topography. The onset of exhumation is set at some time before the oldest AFT age as this timing influences the thermal structure of the crust at the time that AFT ages start being recorded. We have tested two different model configurations: one in which we inverted the data for the Sierra Nevada and El Carmen blocks separately; another one in which the two blocks form part of the same model but are separated by a vertical fault, allowing exhumation rates to vary between the two blocks. The difference is that, in the first case, thermal and topographic parameters are allowed to vary independently between both blocks whereas, in the second case, they are constrained to be similar.

We use the Bayesian Information Criterion (BIC; Schwarz, 1978) for model selection with different numbers of parameters. When estimating model parameters using maximum likelihood estimation, it is possible to increase the likelihood by adding parameters, which may result in over-fitting the data (Glotzbach et al., in review). The BIC resolves this problem by introducing a penalty term for the number of parameters in the model. Thus, we used the following expression:

$$BIC = \frac{1}{\ln\left(L_{\max}\right)^2} + k \cdot \ln(n) \quad (2)$$

where L_{max} is the maximum likelihood achievable for the model ($L = e^{-misfit}$) k is the number of free parameters and n is the number of observations, respectively.

Parameter resolution is assessed by the associated marginal probability density function (PDF), obtained by resampling the model ensemble guided by the posterior probability density function (PPD). Assuming a uniform prior PDF, the log PPD is simply the log-likelihood L.

Table DR3 provides BIC values for inversions with 1 to 4 exhumation phases. Both the separate inversions for the Sierra Nevada and El Carmen blocks and the inversion in which both blocks are combined suggest that the best fit to the data is provided by two exhumation phases in the Sierra Nevada block and a single phase of exhumation in El Carmen. Optimum parameter values (defined by the mean of the 1-D marginal probability density function if it is

symmetric, and by its mode if it is asymmetric) as well as their resolution (1σ standard deviation around the mode) for these model configurations are given in Table DR4; corresponding scatterplots, 1-D and 2-D marginal probability density functions for these two configurations are shown in Figs. DR1 and DR2, respectively. The optimum models are very similar for each configuration, in particular with regards to the exhumation history; we report the values for the combined model in the main text, as that provides the best-resolved and most consistent set of parameters. A comparison between observed age-elevation relationships and those predicted by the optimum combined model is shown in Fig. DR3.

3. Thermal History Modeling

Thermal history modeling was performed using HeFTy v1.3 software (Ketcham, 2005). Input data for the inversions included AFT ages, the AFT track-length distribution (corrected for angle to the C-axis) and D_{par} values calibrated to the values of standard samples used for deriving the annealing model (Ketcham et al., 1999). Models were constrained by the present-day surface temperature and boxes placed around the AFT ages, with box sizes of 5-15 Myr and 60-100 °C so as not to guide thermal histories (cf. Fig. DR4). Random sub-segment spacing was used and no continuous cooling constraint was applied. “Good” and “acceptable” fits to the observations are defined following Ketcham (2005).

References

Barbarand, J., Carter, A., Wood, I., and Hurford, A., 2003, Compositional and structural control of fission-track annealing in apatite: Chemical Geology, v. 198, p. 107-137.

Braun, J., 2003, Pecube: A new finite element code to solve the heat transport equation in three dimensions in the Earth’s crust including the effects of a time-varying, finite amplitude surface topography: Computers and Geosciences, v. 29, p. 787–794.

Braun, J., and Robert, X., 2005, Constraints on the rate of post-orogenic erosional decay from low-temperature thermochronological data: application to the Dabie Shan, China: Earth Surface Processes and Landforms, v. 30, p. 1203-1225.

Carlson, W.D., Donelick, R.A., and Ketcham, R.A., 1999, Variability of apatite fission-track annealing kinetics: I. Experimental results: American Mineralogist, v. 84, p. 1213-1223.

Dunkl, I., 2002, Trackkey: a Windows program for calculation and graphical presentation of fission track data: Computers & Geosciences, v. 28, p. 3-12.

Galbraith, R.F., and Laslett, G.M., 1993, Statistical models for mixed fission track ages: Nuclear Tracks and Radiation Measurements, v. 21, p. 459-470.

Glotzbach, C., van der Beek, P.A., and Spiegel, C., in review, Episodic exhumation of the Mont Blanc massif, Western Alps: constraints from numerical modelling of thermochronology data: Earth and Planetary Science Letters.

Gomez, E., Jordan, T.E., Allmendinger, R.W., and Cardozo, N., 2005, Development of the Colombian foreland-basin system as a consequence of diachronous exhumation of the northern Andes: Geological Society of America Bulletin, v. 117, p. 1272-1292.

Green, P.F., Duddy, I.R., Laslett, G.M., Hegarty, K.A., Gleadow, A.J.W., and Lovering, J.F., 1989, Thermal annealing of fission tracks in apatite 4. Quantitative modelling techniques and extension to geological timescales: Chemical Geology (Isotope Geoscience Section), v. 79, p. 155-182.

Ketcham, R.A., Donelick, R.A., and Carlson, W.D., 1999, Variability of apatite fission-track annealing kinetics: III. Extrapolation to geological time scales: American Mineralogist, v. 84, p. 1235-1255.

Ketcham, R.A., 2005, Forward and inverse modeling of low-temperature thermochronometry data, *in* Reiners, P.W., and Ehlers, T.A., eds., Low-Temperature Thermochronology: Techniques, Interpretations, and Applications: Reviews in Mineralogy and Geochemistry, 58, p. 275-314.

Niu, F., Bravo, T., Pavlis, G., Vernon, F., Rendon, H., Bezada, M., and Levander, A., 2007, Receiver function study of the crustal structure of the southeastern Caribbean plate boundary and Venezuela: Journal of Geophysical Research, v. 112, doi: 10.1029/2006jb004802.

Ojeda, G.Y., 2000, Analysis of Flexural Isostasy of the Northern Andes [PhD thesis]: Miami, FL, Florida International University.

Sambridge, M., 1999a, Geophysical inversion with a neighbourhood algorithm - I. Searching a parameter space: Geophysical Journal International, v. 138, p. 479-494.

—, 1999b, Geophysical inversion with a neighbourhood algorithm - II. Appraising the ensemble: Geophysical Journal International, v. 138, p. 727-746.

Schwarz, G., 1978, Estimating the Dimension of a Model: Annals of Statistics, v. 6, p. 461-464.

Stephenson, J., Gallagher, K., and Holmes, C.C., 2006, A Bayesian approach to calibrating apatite fission track annealing models for laboratory and geological timescales Geochimica Cosmochimica Acta, v. 70, p. 5183–5200.

Valla, P.G., Herman, F., van der Beek, P.A., and Braun, J., 2010, Inversion of thermochronological age-elevation profiles to extract independent estimates of denudation and relief history - I: Theory and conceptual model: Earth and Planetary Science Letters, v. 295, p. 511-522.

Figure captions

Figure DR1. Results of the optimum Pecube-NA inversions shown as scatter diagrams of the misfit between observations and predictions for separate El Carmen and Sierra Nevada block inversions (El Carmen: single exhumation phase – 4 parameters; Sierra Nevada: two exhumation phases – 6 parameters). Model parameters are given in table DR-2. Each dot corresponds to a forward model run, colored according to the model misfit. The black asterisk corresponds to the best-fit model run (lowest misfit value). 1D marginal PDF's of parameter values resulting from the NA-Bayes analysis are plotted along the top and right axes of the plots; 2D marginal PDF's for parameter combinations corresponding to the plots are shown as black and grey contours, corresponding to the 1σ and 2σ confidence levels, respectively. Optimum parameters, corresponding to either the mode or the mean of the 1D marginal PDF's, are reported in table DR-4.

Figure DR2. As Figure DR-1 but for the simultaneous inversion of the Sierra Nevada and El Carmen data (8-parameter model). Model parameters are given in table DR-2; optimum parameters, corresponding to either the mode or the mean of the 1D marginal PDF's, are reported in table DR-4.

Figure D R3. Comparison of observed age-elevation trend for the Sierra Nevada and El Carmen data and the predictions of the optimum model from the simultaneous inversion of both datasets. RMS: root-mean-squared deviation between modeled and observed ages, normalized by the age error.

Figure DR4. Thermal modeling of AFT ages and track-length distributions for samples from the Sierra Nevada, using the HeFTy code (Ketcham, 2005). Results are displayed as time-temperature paths (left diagrams), where green area indicates acceptable fits; pink area indicates good fits; thick black line indicates best fit. Histogram of measured confined track lengths, corrected for angle to the C-axis, is overlain by a calculated probability density function for the best-fit history (right diagrams). Note that modeled t-T paths are well constrained only within the PAZ (yellow band).

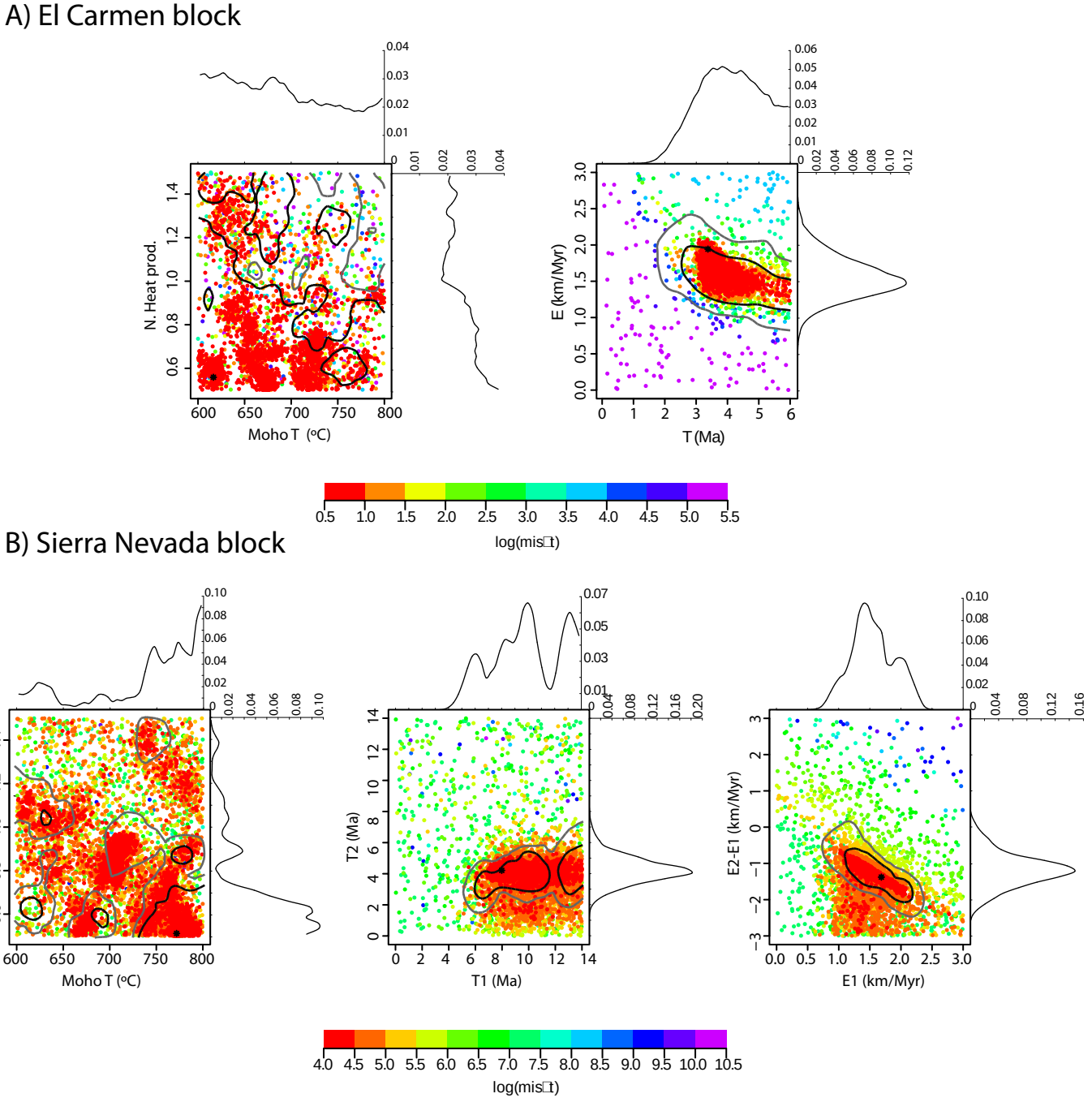

Figure DR-1 Bermúdez et al.

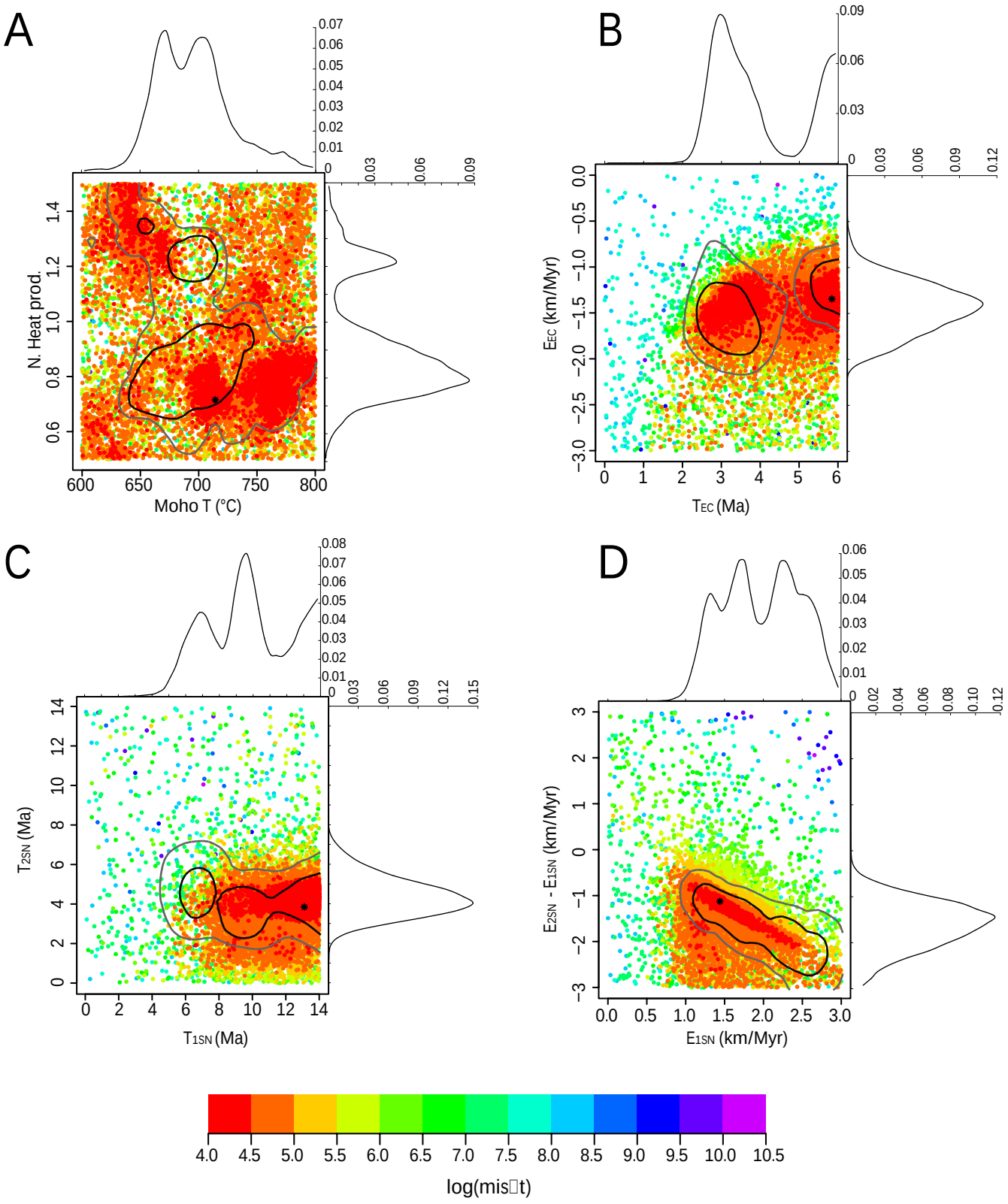

Figure DR-2 Bermúdez et al.

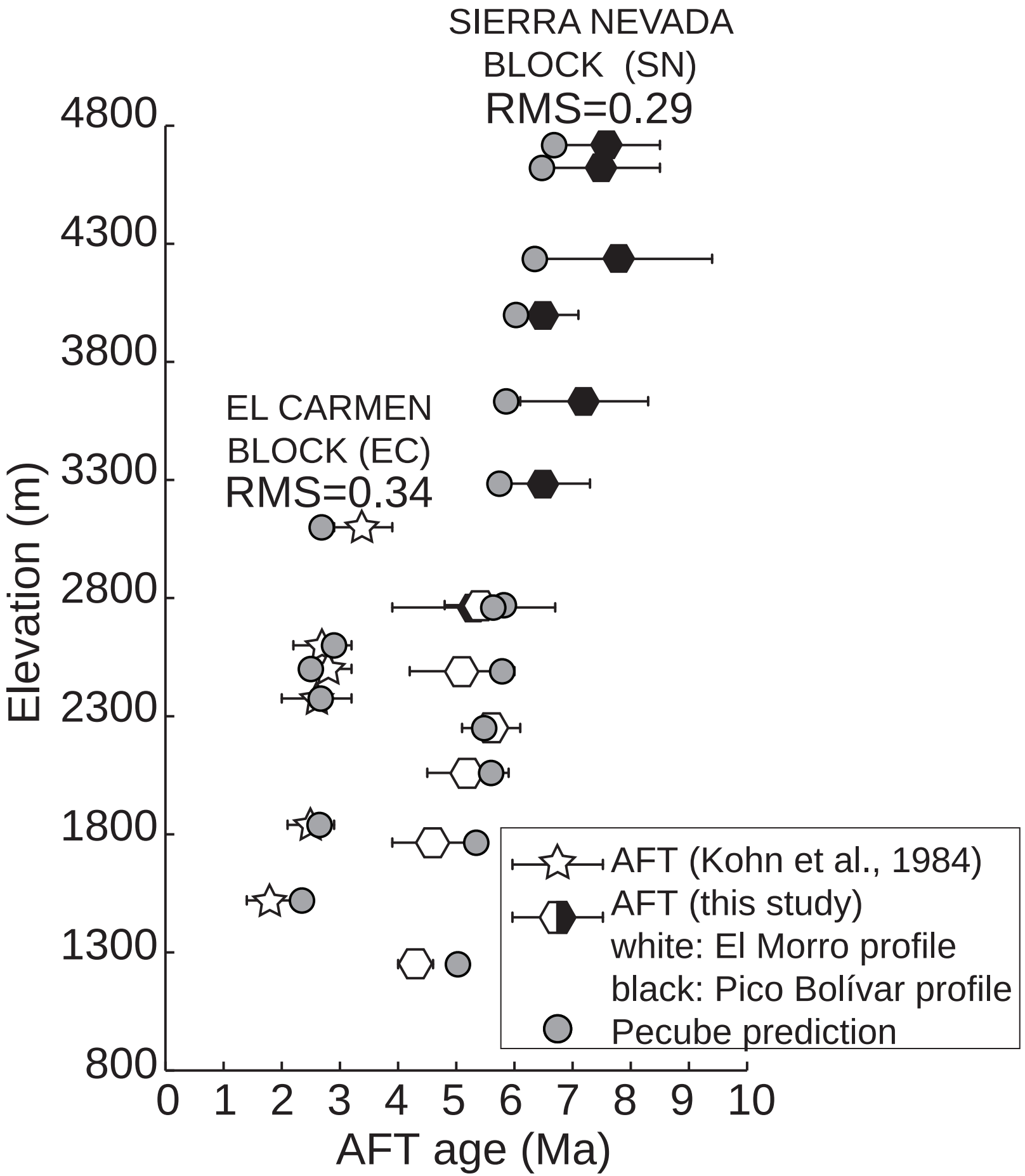

Figure DR-3 Bermúdez et al

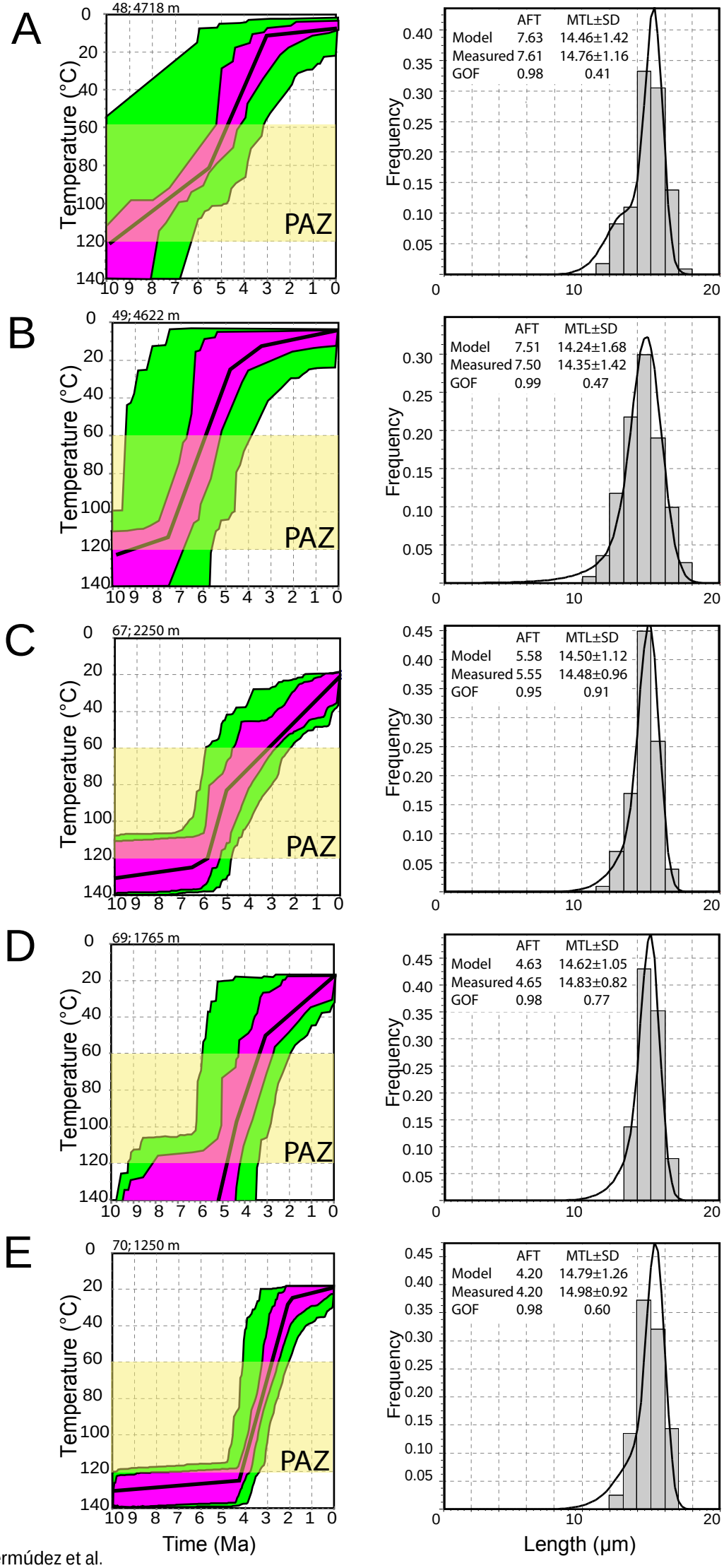

Figure DR-4 Bermúdez et al.

Table DR1: Apatite fission-track data from the Sierra Nevada, central Venezuelan Andes

Sample	Longitude (ºW)	Latitude (ºN)	Elevation (m)	n	ρ_s $\times 10^6$ (cm^{-2})	N_s	ρ_i $\times 10^6$ (cm^{-2})	N_i	ρ_d $\times 10^6$ (cm^{-2})	N_d	$P(\chi^2)$ (%)	D (%)	Age (Ma)	± 1σ	U (ppm)	MTL/ SD (µm)	Dpar/SD (µm)	N
4807	71.0527	8.5317	4718	21	0.082	84	0.924	946	5.950	6656	97.6	0	7.6	0.9	23.4	14.1/1.4	1.4/0.2	108
4907	71.0516	8.5273	4622	24	0.080	61	0.919	697	5.931	6687	99.7	0	7.5	1.0	23.4	14.4/1.4	1.5/0.1	110
5007	71.0790	8.5332	4236	13	0.120	28	1.303	305	5.922	6717	96.6	0	7.8	1.6	28.7	13.9/0.9	1.3/0.1	10
5107	71.0752	8.5437	3999	30	0.071	131	0.935	1729	5.912	6748	99.6	0	6.5	0.6	24.7	14.1/1.3	1.4/0.1	22
5207	71.0826	8.5556	3633	21	0.071	45	0.843	535	5.902	6778	61.8	0	7.2	1.1	21.3	14.4/1.2	1.3/0.1	27
5307	71.0940	8.5700	3285	28	0.038	905	0.500	905	5.893	6809	100	0	6.5	0.8	14.6			
6507	**71.1909 8**	**.4801**	**2770 1**	**8**	**0.284**	**229**	**4.665**	**3760**	**5.873**	**6870**	**0**	**0.4**	**5.4**	**0.6**	**113**			
5407	71.1055	8.5698	2760	11	0.027	16	0.426	255	5.833	6840	99.4	0	5.3	1.4	11.9			
6607	**71.2129 8**	**.4721**	**2490 2**	**0**	**0.035**	**37**	**0.573**	**608**	**5.864**	**6901**	**99.7**	**0**	**5.1**	**0.9**	**16.1**			
6707	**71.2011**	**8.4995**	**2250**	**30**	**0.087**	**174**	**1.316**	**2646**	**5.854**	**6931**	**14.8**	**0.1**	**5.6 0**	**.5 3**	**2.6 1**	**3.9/1.1**	**1.5/0.2**	**100**
6807	**71.1968**	**8.5164**	**2060**	**30**	**0.028**	**61**	**0.450**	**987**	**5.845**	**6962**	**97.1**	**0**	**5.2 0**	**.7 1**	**1.2 1**	**4.0/0.8**	**1.3/0.1**	**15**
6907	**71.2015**	**8.5355**	**1765**	**26**	**0.025**	**52**	**0.451**	**943**	**5.835**	**6993**	**99.9**	**0**	**4.6 0**	**.7 1**	**1.6 1**	**4.4/1.0**	**1.5/0.2**	**51**
7007	**71.2028**	**8.5476**	**1250**	**30**	**0.134**	**320**	**2.689**	**6405**	**5.825**	**7023**	**6.7**	**0.2**	**4.3 0**	**.3 6**	**9.1 1**	**4.5/1.1**	**1.6/0.2**	**118**

Note: Fission-track ages are reported as central ages (Galbraith and Laslett, 1993) using a zeta value of 288.7 ± 5.2 (M. Bermúdez) and the IRMM 540 uranium glass standard. Ages were calculated with the Trackkey program (Dunkl, 2002). Roman numbers represent samples collected along Pico Bolívar profile; bold numbers: El Morro profile. Abbreviations: n = number of grains counted; ρ_s = fossil track density; ρ_i = induced track density; ρ_d = dosimeter track density; N_s, N_i, N_d = number of tracks counted to determine the reported track densities. For irradiations with significant (> 3%) axial gradients in neutron fluence (as monitored by the dosimeters), ρ_d is interpolated between dosimeter values. $P(\chi^2)$ = Chi-square probability that the single grain ages represent one population; D = age dispersion (%); MTL = mean track length; Dpar = Etch-pit width parallel to the C-axis (Carlson et al., 1999; Barbarand et al., 2003); SD = standard deviation of track-length distribution and etch-pit width measurements, respectively; N number of track lengths measured.

Table DR2: Parameter values for the Venezuelan Andes used in *Pecube* modeling. References constraining parameter values are given where appropriate. Parameters in roman font are fixed, the models inverts for parameter values in bold, within the range of values indicated.

Parameter	Reference	Value
	Thermal parameters	
Crustal thickness	(Niu et al., 2007)	40 km
Thermal diffusivity	(Braun and Robert, 2005)	25 km^2
Basal temperature		**600 - 800°C**
Temperature at sea level		25 °C
Atmospheric lapse rate		4 °C km^{-1}
Crustal heat production		**5 - 11 °C Myr^{-1}**
	Flexural parameters	
Crustal density	(Gomez et al., 2005)	2700 kg m^{-3}
Mantle density	(Gomez et al., 2005)	3300 kg m^{-3}
Young's modulus	(Gomez et al., 2005)	70 GPa
Poisson ratio	(Gomez et al., 2005)	0.25
Equivalent elastic thickness	(Ojeda, 2000)	30 km
	Kinematic parameters	
Onset of exhumation SN block		**0 - 14 Ma**
Onset of Exhumation EC block		**0 - 6 Ma**
Initial exhumation rate (both blocks)		**0 – 3 km Myr^{-1}**
Rate change for subsequent exhumation phases (both blocks)		**-3 – 3 km Myr^{-1}**

Table DR3: Bayesian Information Criterion (BIC; Schwartz, 1978) for the different configurations employed in *Pecube* inversion (using fixed topography). Best model for each configuration is shown in bold.

Number of Exh. Phases	Dimension	misfit	Number of observations	BIC	Number of models
		Blocks modeled separately			
		SIERRA NEVADA BLOCK			
1	4	145.57	22	157.93	10100
2 6		**66.63**	**22**	**85.17**	**30100**
3	8	59.75	22	84.48	30100
4	10	59.72	22	90.63	30100
		EL CARMEN BLOCK			
1 4		**1.87**	**6**	**9.03**	**10100**
2	6	1.77	6	12.52	10100
3	8	1.75	6	16.09	10100
4	10	1.53	6	19.44	30100
		Blocks modeled together			
1 SN, 1 EC	6	173.81	28	193.81	10100
2 SN, 1 EC	**8**	**71.03**	**28**	**97.68**	**30100**
2 SN, 2 EC	10	69.76	28	103.08	30100

Table DR4: Parameter inversions for preferred models (indicated in bold in Table DR-3).

Sierra Nevada Block individually

Misfit	BIC	Moho T (°C)	Heat Prod. (°C Myr^{-1})	T_{1SN} (Ma)	E_{1SN} (km Myr^{-1})	T_{2SN} (Ma)	E_{2SN} (km Myr^{-1})
66.63	85.17	738±58	6.7±3.5	10.0±2.6	1.4±0.4	4.0±0.9	0.1±0.5

El Carmen Block individually

Misfit	BIC	Moho T (°C)	Heat Prod. (°C My^{-1})	T_{1EC} (Ma)	E_{1EC} (km Myr^{-1})
1.87	9.03	690±57	10.2±3.1	4.1±1.0	1.5±0.3

Sierra Nevada and El Carmen Blocks simultaneously

Misfit	BIC	Moho T (°C)	Heat Prod. (°C Myr^{-1})	T_{1SN} (Ma)	E_{1SN} (km Myr^{-1})	T_{2SN} (Ma)	E_{2SN} (km Myr^{-1})	T_{1EC} (Ma)	E_{1EC} (km Myr^{-1})
71.03	97.68	696±33	8.6±2.6	9.6±2.5	1.7±0.6	4.0±1.0	0.4±0.5	3.9±1.2	1.4±0.3

NB Optimum parameter values are either the mean or the mode (in case of a strongly asymmetric PDF) of the 1D marginal PDF for each parameter (cf. Figures DR3 and DR4); uncertainty is given as the 1σ standard deviation around the mean or the mode.